Civil Engineering and Applied Solutions
Research Article
journal homepage: ceas.journals.umz.ac.ir

Evaluation of Setting Behavior in Slag-Based Geopolymer Concrete using Ultrasonic Pulse Velocity under Varying Mix Proportions

Nader Sabeti [a*]

[a] *Department of Civil and Architectural Engineering, KTH Royal Institute of Technology, Stockholm, Sweden*

ARTICLE INFO

Keywords:
Sustainable development
Geopolymer concrete
Slag-based binder
Setting time
Ultrasonic pulse velocity (UPV) method
Freshcon mold system

Article history:
Received 03 July 2025
Accepted 23 July 2025
Available online 01 August 2025

ABSTRACT

In response to the growing environmental crisis and the urgent need to curb carbon emissions and improve waste management, slag-based geopolymer concrete has emerged as a low-energy, sustainable alternative to ordinary Portland cement. This study investigates the initial and final setting behaviour of ground-granulated blast-furnace slag (GGBFS) geopolymer concrete using the ultrasonic pulse velocity (UPV) technique alongside a Freshcon mold system. Key variables examined include the molarity and type of alkaline activator, the alkali-to-slag ratio, and the proportion of slag within the concrete matrix. UPV traces delineate three distinct stages of induction (dormant), polymerization onset (activation), and network consolidation (hardening), each typified by its signature "S-shaped" profile. In this study, increasing the concentration of the alkaline activator and the proportion of ground granulated blast-furnace slag (GGBFS) was found to dramatically shorten both initial and final setting times of slag-based geopolymer mixtures; however, beyond an optimal activator concentration and solution-to-slag ratio, these accelerating effects attenuate and polymerization kinetics become disrupted. Notably, whereas ordinary Portland cement exhibits an induction period over 240 minutes, geopolymer samples activated at 6M complete their induction phase in under 30 minutes, a 6–8 fold increase in initial setting rate. Such rapid setting, while advantageous for expediting placement cycles, poses challenges in mass concrete pours by heightening the risk of cold joints and imposing stringent formwork time constraints. Conversely, this accelerated hardening can be leveraged as a significant asset in future investigations into precast concrete elements and tunnel-lining shotcrete applications.

1. Introduction

Geopolymer concrete, as a pioneering innovation in sustainable construction materials, has been developed to reduce greenhouse gas emissions and make optimal use of industrial by-products [1-3]. CO_2 emissions from Portland cement production amount to approximately 0.8–1.0 tonnes per tonne of cement, representing over 7–8% of total global emissions [4, 5]. In contrast, life-cycle assessments of blast-furnace slag–based geopolymer concrete show that its CO_2 emissions are 65–75% lower than those of Portland cement concrete [6]. Moreover, the use of slag as a precursor converts steelmaking waste into a valuable source of silica and calcium, thereby reducing industrial residues and conserving natural resources [1, 7]. In other words, geopolymer concrete not only exhibits a reduced carbon footprint but also contributes effectively to CO_2 sequestration and energy savings during material production [3, 4]. Recent studies have demonstrated that, during the alkaline activation process, recovering waste heat energy and maximizing the sodium silicate-to-hydroxide ratio can further reduce carbon emissions by up to 80%. This exceptional environmental potential renders geopolymer concrete an attractive option for low-carbon structural projects and climate-sensitive regions [1, 2].

The chemical behavior of blast-furnace slag–based geopolymer concrete is governed by geopolymerization reactions [8-10].

---

* Corresponding author.
E-mail addresses: sabeti@kth.se (N. Sabeti).

https://doi.org/10.22080/ceas.2025.29600.1023
ISSN: 3092-7749/
How to cite this article: Sabeti, N. Evaluation of Setting Behavior in Slag-Based Geopolymer Concrete using Ultrasonic Pulse Velocity under Varying Mix Proportions. Civil Engineering and Applied Solutions. 2025; 1(3): 48–61. doi:10.22080/ceas.2025.29600.1023.

Iron-smelting slag comprises a mixture of glassy and crystalline phases, namely C_2S, C_3S, the Mg–Fe solid solution, and various silicate phases [7]. In the presence of strong alkaline activators and alkali silicates, the amorphous silica–alumina network rapidly dissolves, releasing SiO_4^{4-} and AlO_4^{5-} monomers [10-13]. These anions then coordinate with Na^+ or K^+ cations in solution to form densely cross-linked –Si–O–Al–O– polymer chains, which evolve into N–A–S–H gels within the macromolecular matrix [9, 11, 14]. Concurrently, the abundant Ca^{2+} in the slag fosters the co-precipitation of C–A–S–H alongside N–A–S–H, yielding a dual-gel microstructure with enhanced mechanical performance [15, 16]. The Si/Al and Ca/Si ratios critically influence polymerization kinetics, pore structure, and crystalline phase development [17]. Moreover, the silicate modulus (Na_2SiO_3/NaOH ratio) and the activator concentration dictate the gel's microstructural characteristics: a higher silicate modulus promotes increased silica chain length and network connectivity, thereby reducing permeability [18, 19].

The rheological properties and setting time of fresh concrete are critical factors that influence its workability, durability, early-age bond strength, and suitability for various construction applications, including mass concrete pouring, precast element fabrication, and shotcrete use for tunnel support [20-22]. Traditional shotcrete formulations, for example, typically rely on Portland cement with a high clinker content to achieve the rapid setting required for effective shotcrete tunnel lining [22]. However, the use of Portland cement often necessitates the application of thicker layers, leading to increased consumption and a subsequent rise in environmental impacts [5, 6]. Consequently, there is a pressing need for further research to identify and develop sustainable alternative materials, such as geopolymers, which can deliver comparable performance while mitigating environmental effects [3].

Previous studies have demonstrated that the setting time of geopolymer concrete is influenced by a range of factors, including the type of raw material, the type of alkaline activator, the molar concentration of the activator, the alkali-to-raw material ratio, ambient temperature during mixing, and several other variables [23-25]. Both the type of alkali activator (NaOH vs. KOH) and its concentration profoundly affect paste behavior [18, 24]. Specifically, increasing the molarity of hydroxide solutions elevates mixture viscosity and thereby reduces workability, while simultaneously accelerating the polymerization rate in fly-ash–based geopolymers [26]. Comparative analyses indicate that KOH, owing to the larger ionic radius of K^+, enhances the dissolution of aluminosilicate species and generates a more open gel network, which translates into comparatively better initial flowability than NaOH-activated systems. In addition, raising the sodium silicate content markedly increases viscosity and diminishes the flowability of the fresh geopolymer paste [15].

Determination of initial and final setting times in geopolymer concrete conventionally follows ASTM C403, which employs a series of standardized penetrometer measurements [27]. However, needle-penetration methods are inherently operator-sensitive and exhibit diminished reliability under elevated curing temperatures [28]. To overcome these limitations, ultrasonic pulse-velocity (UPV) monitoring has been advanced as a non-destructive, high-precision alternative [29, 30]. In UPV testing, time-resolved records of decreasing ultrasonic wave velocity and concomitant increases in material stiffness reflect the progression of geopolymerization and delineate both the initial and final set points [23, 29]. This technique has demonstrated exceptional repeatability and sensitivity, particularly at temperatures above ambient and when assessing the influence of varied alkali activator chemistries, thereby enabling more accurate characterization of setting kinetics in geopolymer systems [24, 28].

Given that previous investigations have employed ultrasonic pulse-velocity (UPV) solely to evaluate the setting kinetics of ordinary Portland cement and no systematic data exist on how varying alkali-activator concentrations affect the setting behavior of slag-based geopolymers, this study applies UPV to accurately characterize the initial and final setting times of fresh geopolymer concrete.

2. Experimental preparation

2.1. Material properties

Fine and coarse aggregates used for specimen preparation were sourced from a nearby fluvial deposit and rigorously characterized per the applicable standards. Particle-size distribution curves, obtained via sieve analysis per ASTM C136 [31], are shown in Fig. 1. The fine aggregate exhibited a saturated surface dry (SSD) bulk specific gravity of 2.65, a fineness modulus of 3.7, and a maximum nominal particle size of 12 mm. The coarse aggregate displayed an SSD bulk specific gravity of 2.64 and was thoroughly washed on-site to remove adhering fines and impurities prior to mix preparation [32].

Blast-furnace slag used in this study is the by-product of the basic oxygen furnace (BOF) steelmaking process. In the BOF route, molten iron derived from iron ore or scrap is charged into the furnace together with fluxing agents such as lime or dolomite. High-pressure oxygen is then blown in to oxidize impurities, which separate as gaseous species and metallic oxides. Upon tapping of the purified steel, the residual slag, composed predominantly of silicates and metal oxides (CaO, SiO_2, Al_2O_3), is recovered. Chemically analogous to Portland cement, this solidified material finds widespread application in the production of slag cements, concrete aggregates, railroad ballast, road subbases, and refractory products.

In this study, Type II Portland cement obtained from a domestic cement works and BOF slag procured from a regional steel producer were employed. The precise chemical compositions of both materials are listed in Table 1, and Fig. 2 presents photographs of the slag alongside the ceramic powder utilized.

In the formulation of geopolymer concretes, the selection of alkali activator, either NaOH or KOH, exerts a profound effect on the microstructure and mechanical properties of the hardened matrix. Although both Na^+ and K^+ possess the same charge, the smaller ionic radius of Na^+ promotes tighter ion-pairing with silicate oligomers, leading to accelerated geopolymerization kinetics but a comparatively less dense gel network.

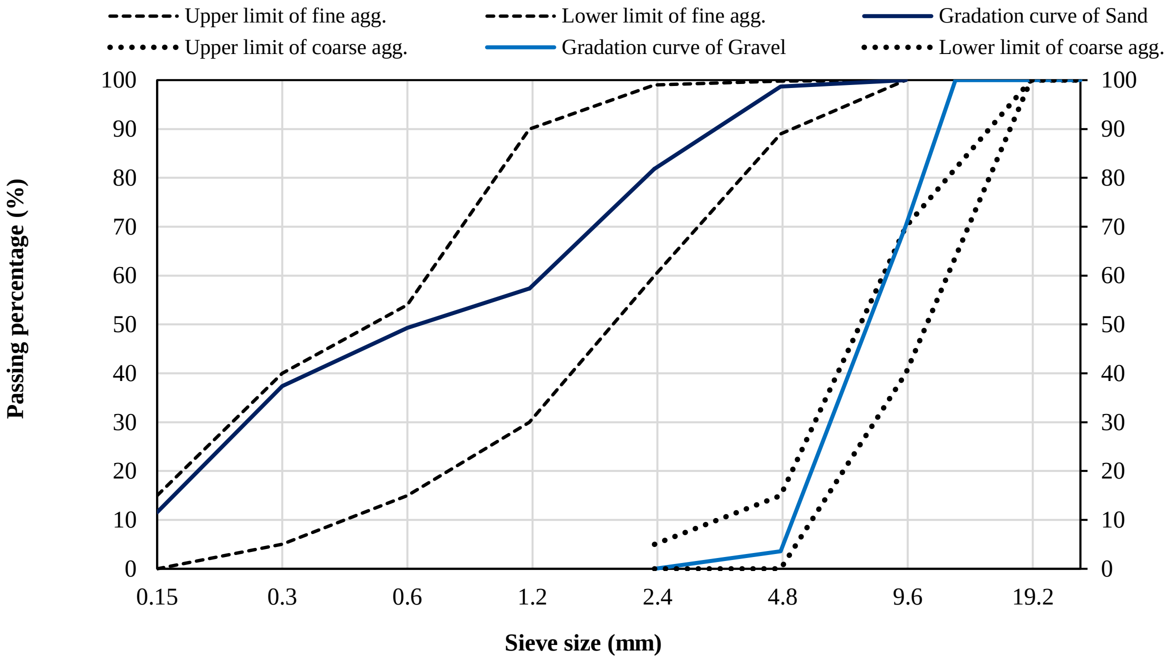

Fig. 1. Grading graph of the fine and coarse aggregates.

Table 1. Chemical analysis of cementing materials.

Type	**Chemical Compound (%)**										
	CaO	**SiO_2**	**Al_2O_3**	**Fe_2O_3**	**SO_3**	**MgO**	**Na_2O**	**K_2O**	**TiO_2**	**MnO**	**L.O.I**
Slag	38.32	32.09	15.12	1.23	2.28	7.75	0.42	0.47	1.23	0.99	0.02
Portland cement	64.79	19.99	4.95	3.43	3.12	1.72	0.39	0.61	0.7	-	0.96

Conversely, the larger K^+ favors the formation of bulkier silicate oligomers and thus a denser gel phase, which enhances compressive strength [33].

Fig. 2. Photographs of the (a) blast-furnace slag, and (b) ceramic powder used in the geopolymer concrete mixtures.

Nevertheless, balancing economic and processing considerations, a NaOH concentration of 4–8 M is generally identified as optimal; concentrations above ~10 M not only plateau strength gain but can also induce efflorescence and embrittlement in the geopolymer matrix. Furthermore, a SiO_2/Al_2O_3 molar ratio in the range of 3.3–6.5 is recommended to establish an ideal three-dimensional aluminosilicate network [23]. Figs. 3 and 4 show the NaOH and KOH activator solutions employed in this study.

Fig. 3. Sodium hydroxide (NaOH) flakes used as the alkaline activator in the geopolymer concrete formulation.

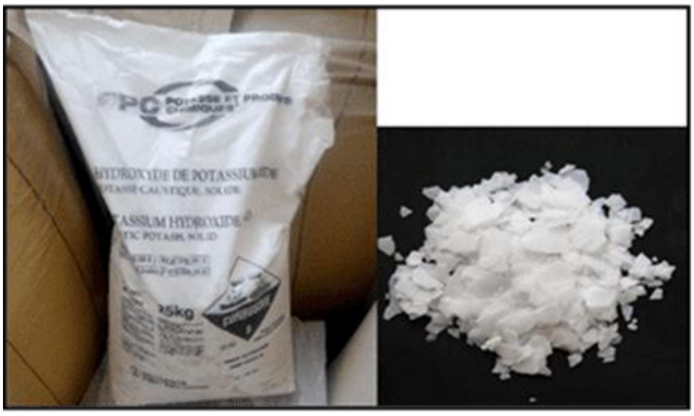

Fig. 4. Potassium hydroxide (KOH) flakes used as the alkaline activator in the geopolymer concrete formulation.

The most critical characteristic of sodium silicate solution (water glass) is its SiO_2/Na_2O molar ratio, which in commercial products typically ranges from 1.5 to 3.2. In general, higher-ratio silicates are more suitable for chemical bonding because the siliceous fraction more readily reacts with cations. However, to maintain a high alkaline concentration while activating pozzolanic materials, lower-ratio silicates are recommended [34]. In the present study, a sodium silicate solution with an SiO_2/Na_2O molar ratio of 2.45 was employed for geopolymer synthesis.

2.2. Mix design

The mix design for the geopolymer concrete series was established by maintaining a fixed sodium silicate-to-caustic soda (NaOH) mass ratio of 2.5. Three alkali-to-slag ratios, 0.4, 0.45, and 0.5, were selected to elucidate the effect of activator dosage on fresh-state rheology and hardened-state strength. In parallel, NaOH solution molarities of 4 M, 6 M, and 8 M were employed to investigate the influence of hydroxide concentration on geopolymerization kinetics and microstructural development. The proportions for the control ordinary Portland cement concrete mix are tabulated in Table 2, while the corresponding geopolymer formulations appear in Table 3.

To assess the impact of mixing sequence on geopolymer performance, two distinct protocols were implemented:

- Simultaneous-addition protocol (Protocol I): The NaOH and sodium silicate solutions were thoroughly blended before their introduction to the slag binder.
- Staged-addition protocol (Protocol II): The NaOH solution was first combined with the slag and allowed to interact for a predefined induction period; subsequently, the sodium silicate was incorporated, and finally, the resulting paste was mixed with the aggregate fraction.

Compressive strength testing at 28 days revealed no statistically significant difference between Protocol I and Protocol II. This finding corroborates the mechanistic understanding that initial alkali attack on the aluminosilicate framework cleaves Al–O–Si bonds to release reactive oligomers, which then condense into a cohesive C–A–S–H–type gel upon contact with silicic species from the sodium silicate [17]. Nonetheless, the staged-addition approach is recommended in practical applications to avoid direct, prolonged exposure of aggregates to high-pH activator solutions, thereby mitigating the risk of deleterious alkali–aggregate reactions and ensuring an optimal interfacial transition zone between binder and aggregate.

Table 2. Mix proportions of OPC specimens.

Mix ID	Component					
	Coarse agg. (kg/m^3)	Fine agg. (kg/m^3)	Cement (kg/m^3)	Water (kg/m^3)	W/C	Slump (mm)
OPC-Code-01	519	1209	400	180	0.4	95
OPC-Code-02	506	1182	400	200	0.5	108

3. Experimental procedure

3.1. Setting time characterization of fresh geopolymer concrete

The early-stage development of the geopolymer's microstructure exerts a decisive influence on its mechanical performance, physical integrity, and long-term durability. Geopolymerization commences when alkaline activators react with aluminosilicate precursors, forming a cohesive inorganic polymer network that dictates the material's behavior in the initial hours post-mixing. In this fresh state, the geopolymer paste exhibits high plasticity and workability, facilitating critical operations such as mixing, transportation, and placement.

Table 3. Mix proportions of geopolymer concrete specimens.

Mix ID	Component											
	Coarse agg. (kg/m^3)	Fine agg. (kg/m^3)	NaOH	KOH	Activator water	Na_2SiO_3	Slag (kg/m^3)	Alk/Slag	Extra water	Molarity	SH/SS	Ceramic (kg/m^3)
AAS.1	519	1209	16.4	-	98	45.7	400	0.4	65	4	2.5	-
AAS.2	519	1209	23.4	-	90.9	45.7	400	0.4	65	6	2.5	-
AAS.3	519	1209	30	-	84	45.7	400	0.4	65	8	2.5	-
AAS.4	512	1196	18.4	-	110.2	51.4	400	0.45	65	4	2.5	-
AAS.5	512	1196	24.4	-	102.2	51.4	400	0.45	65	6	2.5	-
AAS.6	512	1196	33.7	-	94.9	51.4	400	0.45	65	8	2.5	-
AAS.7	506	1182	20.4	-	122.5	57.2	400	0.5	65	4	2.5	-
AAS.8	506	1182	29.3	-	113.6	57.2	400	0.5	65	6	2.5	-
AAS.9	506	1182	37.5	-	105.4	57.2	400	0.5	65	8	2.5	-
AAS.11	506	1064	29.3	-	113.6	57.2	400	0.5	65	6	2.5	118.2
AAS.12	519	1209	-	22.3	92	45.7	400	0.4	65	4	2.5	-
AAS.13	512	1196	-	25.1	103.5	51.4	400	0.45	65	4	2.5	-
AAS.14	506	1182	-	27.9	115	57.2	400	0.5	65	4	2.5	-
AAS.15	529	1235	25.7	-	99.4	50	350	0.5	65	6	2.5	-
AAS.16	484	1128	33	-	127.8	64.3	450	0.5	65	6	2.5	-

As polymerization advances, the paste undergoes progressive stiffening—a phenomenon referred to as setting. The initial setting time defines the duration during which the material retains adequate plasticity and deformation capacity, whereas the final setting time marks the onset of rigidity and the development of measurable mechanical strength. Precise determination of these intervals is essential for optimally scheduling formwork installation, compaction, surface finishing, and formwork removal, as well as for the judicious selection of chemical admixtures (accelerators or retarders) tailored to project requirements. Standardized test methods for quantifying setting behavior in fresh geopolymer and cementitious systems include the Vicat needle penetration test (ASTM C191 [35]), the penetration resistance method (ASTM C403 [27]), and ultrasonic pulse velocity monitoring (BS 1881 [36]).

In the ultrasonic pulse-velocity method, the setting progression of fresh geopolymer concrete (or hydration in Portland cement) can be delineated by the S-shaped velocity-time curve (Fig. 5) and corresponding schematic microstructural illustrations (Fig. 6) across three distinct phases:

Dormant Phase (A → B): Immediately after mixing, pulse velocity remains low and nearly constant (below ~600 m/s), as cement grains or aluminosilicate precursors are dispersed within the aqueous medium and entrapped gas bubbles (Fig. 6a). Up to point B, gradual dissolution of fine particles and surface coating of larger grains commences, giving rise to nascent solid clusters (Fig. 6b), yet no continuous propagation path exists for the ultrasonic waves.

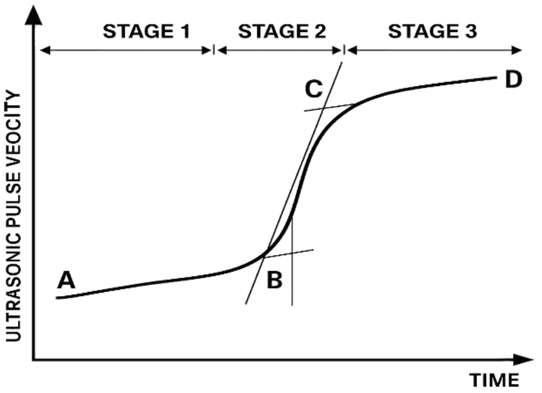

Fig. 5. Schematic illustration of UPV monitoring during the setting stages of fresh geopolymer concrete [37].

Acceleration Phase (B → C): With the formation of aluminosilicate gel products (e.g., ettringite analogues) and the development of an interconnected structural network (Fig. 6c), pulse velocity rapidly increases from approximately 600 m/s to more than 3,500 m/s—corresponding to the onset of measurable mechanical strength.

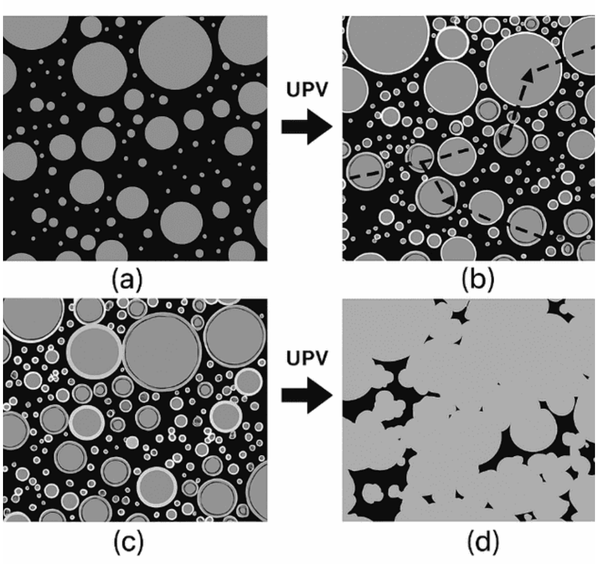

Fig. 6. Microstructural evolution from dispersed particles to a continuous solid network.

Deceleration Phase (C → D): Upon the completion of particle binding and the filling of capillary pores with hydrated reaction products (Fig. 6d), the pulse velocity gradually approaches its asymptotic maximum, signifying the near-end of major structural reactions.

3.2. Fabrication of the ultrasonic setting test mold

The apparatus used to determine concrete setting time by the ultrasonic method—allowing wave-velocity measurements at arbitrary intervals immediately after casting was built by the system introduced by Reinhardt and Grosse [38], first realized at the University of Stuttgart in 2000 (see schematic in Fig. 7). The so-called "Freshcon" mold consists of two PMMA (acrylic) plates, each measuring 15 × 200 × 500 mm, mounted parallel to one another at a separation of 120 mm utilizing four steel shafts. To ensure that ultrasonic pulses do not bypass the specimen at the edges, the plates are sufficiently long, and a U-shaped rubber sponge (30 × 120 × 500 mm) is inserted between them; this sponge minimizes wave scattering inside the mold. Each plate is drilled at its center to accommodate the transmitting and receiving ultrasonic transducers, which are inserted through these holes and brought into contact with the plate surfaces. Ultrasonic measurements were then carried out using a PUNDIT device (fundamental frequency 54 kHz) every 5 minutes during the first hour after casting, and subsequently at 15-minute intervals.

The transmitting transducer was placed in direct contact with the Plexiglas plate and aligned through the full thickness of the concrete specimen, as shown in Fig. 7. After traversing the concrete, the ultrasonic vibrations were captured by the receiving transducer, which was similarly coupled to the opposite Plexiglas surface. The receiver measured the transit time of the pulsed waves through the specimen; by dividing the known path length (i.e., the straight-line distance between the transducers) by this measured time, the ultrasonic pulse velocity was obtained. This technique is applicable not only for determining setting characteristics, compressive strength, and elastic modulus of concrete, but also for assessing durability parameters—such as crack detection and damage evaluation.

Ultrasonic pulse velocities were recorded using a PUNDIT system following BS 1881 [36]. Fig. 8 illustrates the laboratory arrangement of the PUNDIT apparatus, equipped with 54 kHz transducers and a calibrated Plexiglas reference cylinder. The geometrical and acoustic properties of this cylinder are precisely known, and it is employed before each test to zero the instrument via the variable-delay control unit.

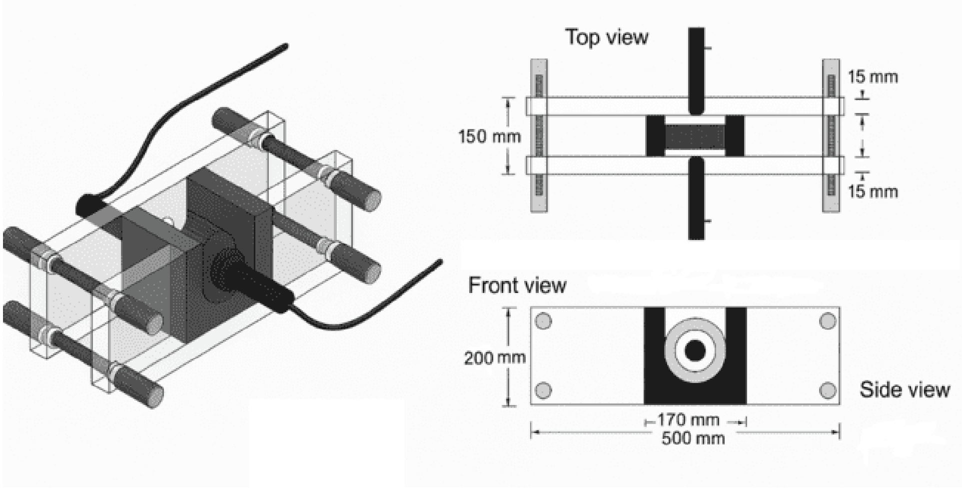

Fig. 7. Schematic diagram of the Freshcon mold with key dimensions (in mm) for fresh-state testing.

The pulse velocity, V, was calculated using Eq. 1:

$$V = \frac{L}{\Delta \mathrm{t}} \tag{1}$$

where L is the distance between transducer faces and Δt is the measured transit time.

Fig. 8. Calibration of the PUNDIT device.

4. Results and discussions

As illustrated in Fig. 9, ultrasonic waves are transmitted from one probe into the fresh concrete mold and received by the opposing probe. The wave transit time is recorded at predetermined intervals with microsecond precision. Using Eq. 1, the pulse velocity is then calculated. Finally, the velocity–time profile is plotted for each concrete sample, enabling a non-destructive rheological assessment of the concrete's structural evolution over time.

According to the UPV curves in Figs. 10 to 12, raising the NaOH molarity from 4 M to 8 M markedly accelerates the early hardening of geopolymer concrete. For example, at an alkali-to-slag ratio of 0.4 (Fig. 10), the 30-minute UPV values for AAS.1 (4 M), AAS.2 (6 M), and AAS.3 (8 M) were all approximately 600 m/s. After 120 minutes, these rose to roughly 970 m/s, 1,700 m/s, and 2,500 m/s, respectively, and by 180 minutes reached 1,240 m/s, 2,800 m/s, and 3,550 m/s. By 360 minutes, AAS.2 and AAS.3 approached their plateau velocities of about 4,200–4,280 m/s, whereas AAS.1 attained only ≈2,000 m/s. The steeper velocity increases with higher OH^- concentration reflect more rapid aluminosilicate dissolution and N–A–S–H gel formation, confirming hydroxide concentration as the principal factor in shortening both initial and final setting phases [7, 39].

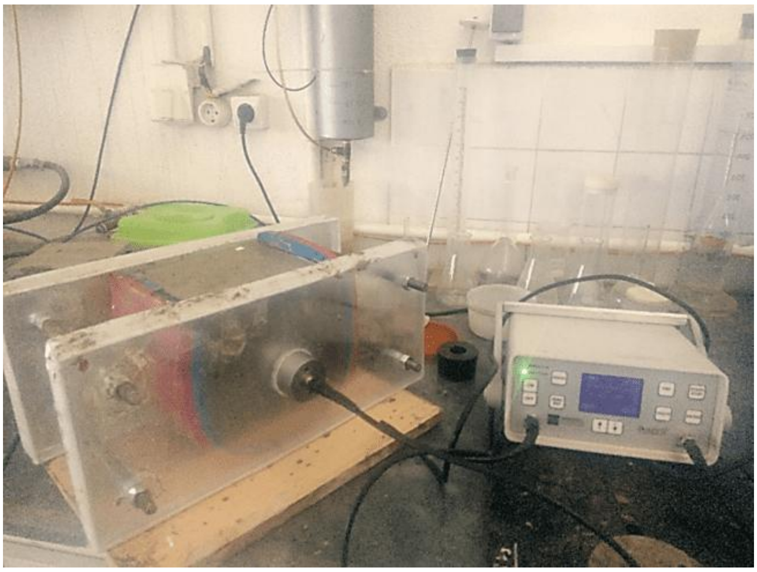

Fig. 9. UPV testing of fresh concrete using the Freshcon mold and PUNDIT device.

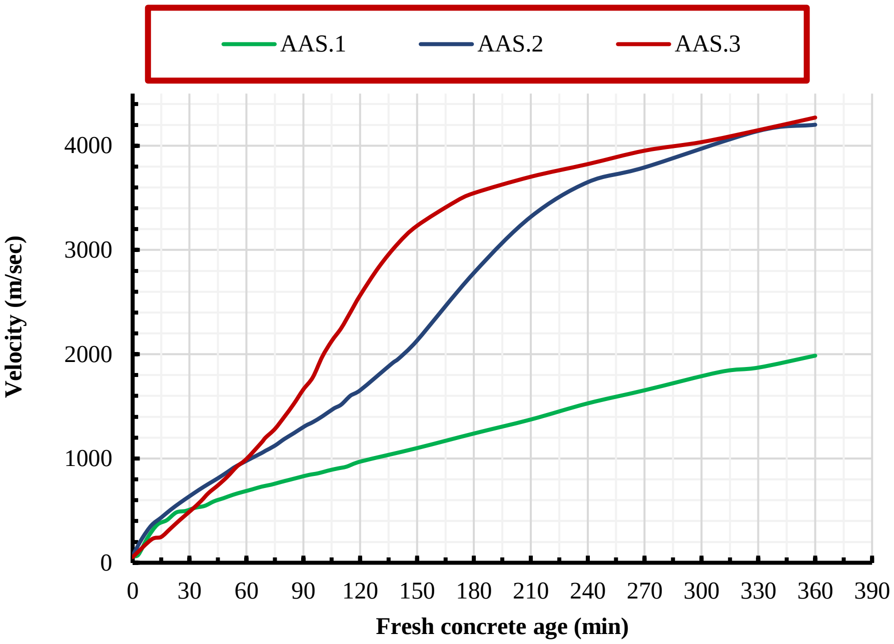

Fig. 10. Effect of NaOH solution molarity on the setting-time curve of concrete with an alkali-to-slag ratio of 0.4.

In Figs. 13 to 15, increasing the total dosage of the alkaline activator accelerates the heat evolution reaction and shortens the induction period, indicating more rapid slag dissolution and earlier formation of C–(A)–S–H gels [40]. This behavior is mechanistically attributed to the expedited removal of Ca^{2+} ions from the pore solution, which amplifies the concentration gradient between the slag surface and the aqueous phase, thereby promoting further slag dissolution and faster gel precipitation [41]. Meanwhile, by maintaining a constant silica-to-alkali modulus (SiO_2/Na_2O) across all tests, the study isolates the effect of total alkali and silicate ion content on reaction kinetics [40, 42].

Fig. 16 compares the setting-time profiles of geopolymer concretes activated with 4 M NaOH versus 4 M KOH. The markedly accelerated setting observed in the KOH-activated system can be attributed to the distinct physicochemical properties of the K^+ ion: its lower hydration enthalpy (≈–322 kJ/mol compared to –406 kJ/mol for Na^+) results in a more labile hydration shell that releases OH^- more readily for C–(A)–S–H gel formation. Furthermore, the larger ionic radius of K^+ (1.38 Å vs. 1.02 Å for Na^+) reduces the structuring of its solvation sphere and lowers the viscosity of the activator solution, thereby enhancing the diffusivity of alkali and dissolved slag species [43]. This increased ionic mobility expedites the depolymerization of the aluminosilicate network and the nucleation of gel phases, culminating in a pronounced reduction of both initial and final setting times.

Fig. 17 illustrates the effect of varying ground-granulated blast-furnace slag (GGBFS) dosages on the setting behavior of geopolymer concrete mixtures. As anticipated, increasing the slag content from 350 kg/m³ (AAS.15) to 450 kg/m³ (AAS.16) accelerates hydration reactions and reduces both initial and final setting times. This enhancement is driven by the additional calcium provided by the slag, which markedly promotes C–S–H and C–A–S–H gel formation. Consequently, higher slag proportions yield more rapid gel nucleation and growth, resulting in faster stiffening of the geopolymer matrix.

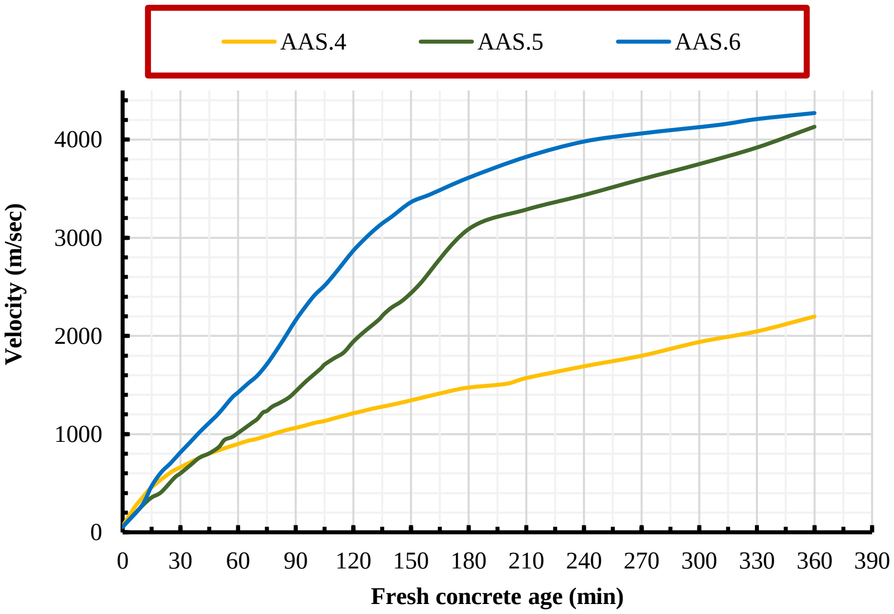

Fig. 11. Effect of NaOH solution molarity on the setting-time curve of concrete with an alkali-to-slag ratio of 0.45.

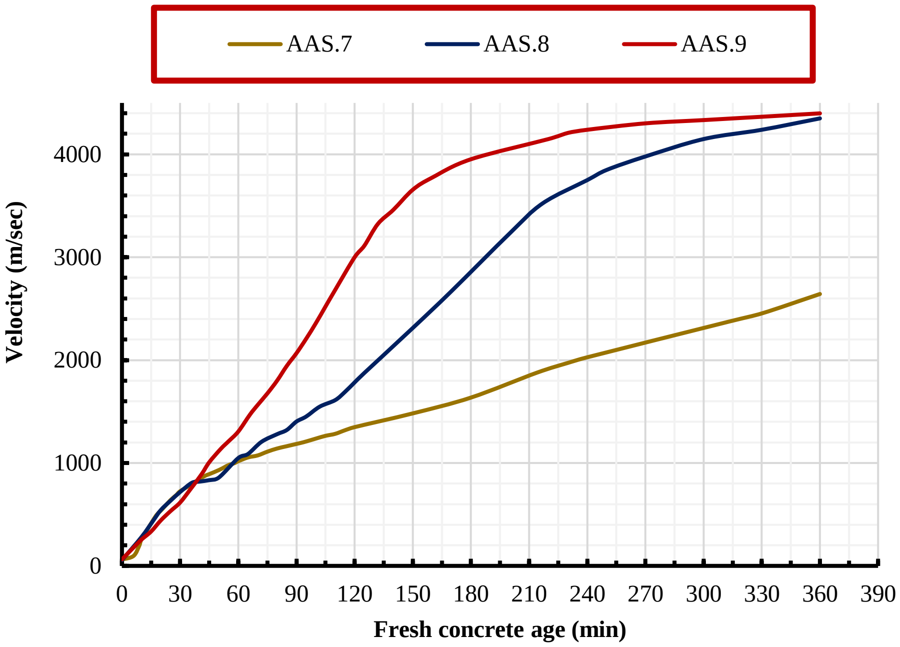

Fig. 12. Effect of NaOH solution molarity on the setting-time curve of concrete with an alkali-to-slag ratio of 0.5.

Fig. 18 examines the effect of substituting 10 wt.% of natural fine aggregate with ceramic tile waste powder in the geopolymer blend. The results demonstrate that this level of replacement exerts no discernible influence on the setting kinetics of the geopolymer concrete.

Fig. 19 presents a comparative analysis of the setting behavior of the investigated geopolymer mixtures versus ordinary Portland cement (OPC) concretes. The ultrasonic pulse-velocity profiles reveal that all geopolymer samples (AAS.1 through AAS.16) enter both initial and final setting phases markedly earlier than the OPC references (OPC-Code-01, OPC-Code-02, and CEM I 42.5 [44]). On average, the onset of the sharp velocity increase commonly taken as the initial set threshold of approximately 1,000 m/s occurs between 20 and 50 minutes after casting for the geopolymer specimens, whereas none of the OPC samples reach this velocity even after 240 minutes. For instance, OPC-Code-01 and OPC-Code-02 attain 1,000 m/s at roughly 300 minutes and 360 minutes, respectively, while CEM I 42.5 reaches this stage between 200 and 220 minutes. Final setting indicated by pulse velocities in the 3,000–3,500 m/s range, and the commencement of the tertiary slope occurs for geopolymer concretes between 90 and 180 minutes, with most AAS mixtures stabilizing near 3,500–4,000 m/s in under 3 hours. In contrast, OPC-Code-01 requires approximately 12 hours (720 minutes) to reach 3,500 m/s, OPC-Code-02 about 13–14 hours (780–840 minutes), and CEM I 42.5 around 10 hours (600–650 minutes). Thus, the geopolymer systems demonstrate polymerization and hardening rates that are on average 5–8 times faster than those of ordinary Portland cement concretes.

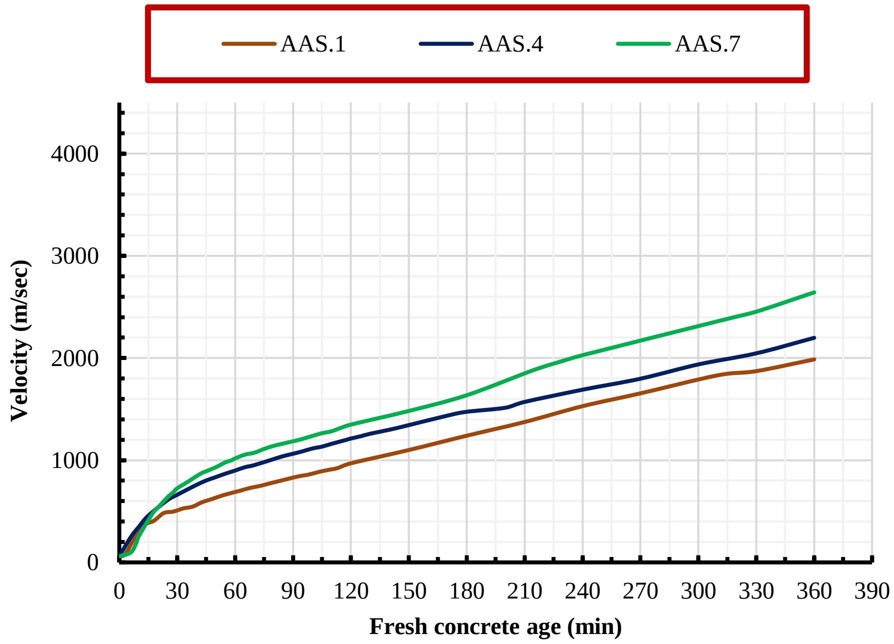

Fig. 13. Setting-time curves for geopolymer concrete with varying alkali-to-slag ratios activated by 4 M NaOH.

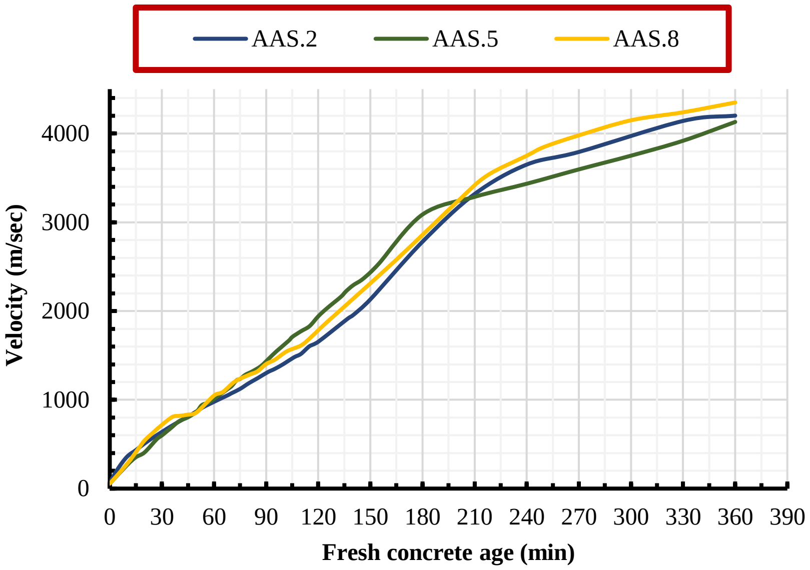

Fig. 14. Setting-time curves for geopolymer concrete with varying alkali-to-slag ratios activated by 6 M NaOH.

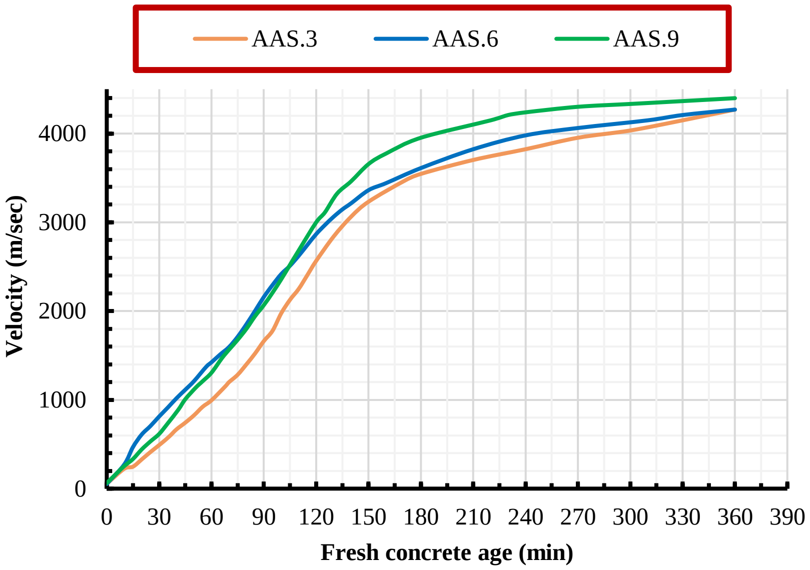

Fig. 15. Setting-time curves for geopolymer concrete with varying alkali-to-slag ratios activated by 8 M NaOH.

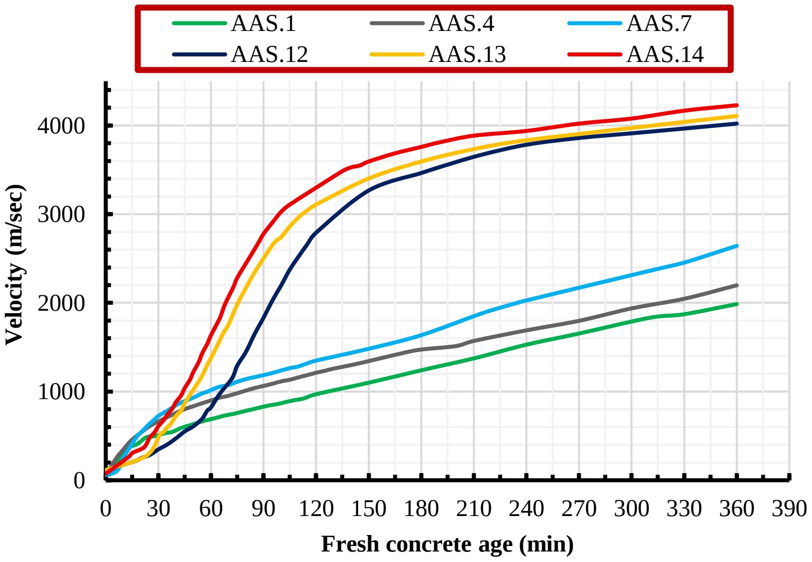

Fig. 16. Comparison of setting-time curves for geopolymer concrete activated with different alkaline solutions.

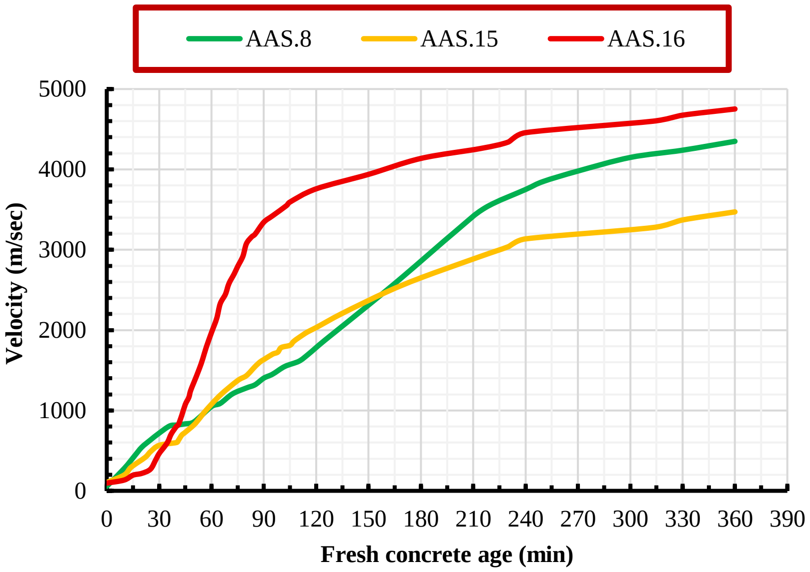

Fig. 17. Setting-time curves of geopolymer concrete mixtures with varying GGBFS contents.

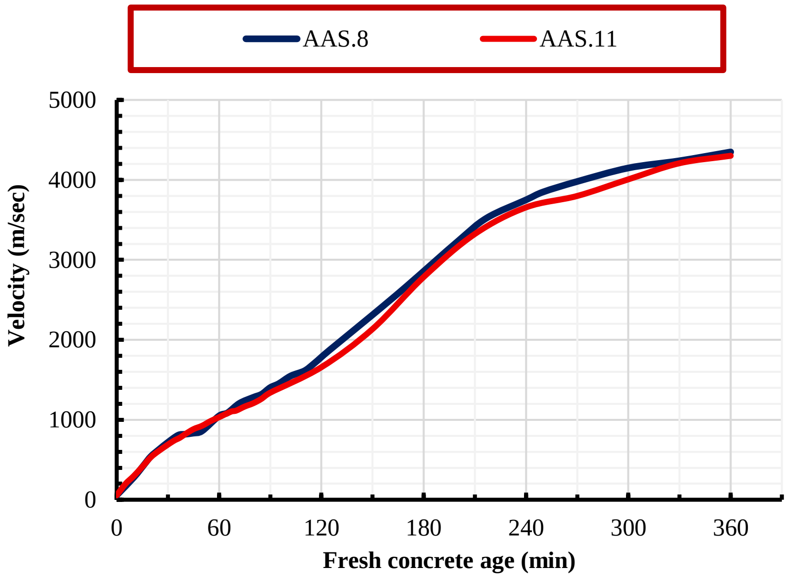

Fig. 18. Comparison of setting-time curves between the reference mix and the mix with 10% ceramic tile powder replacing fine aggregate.

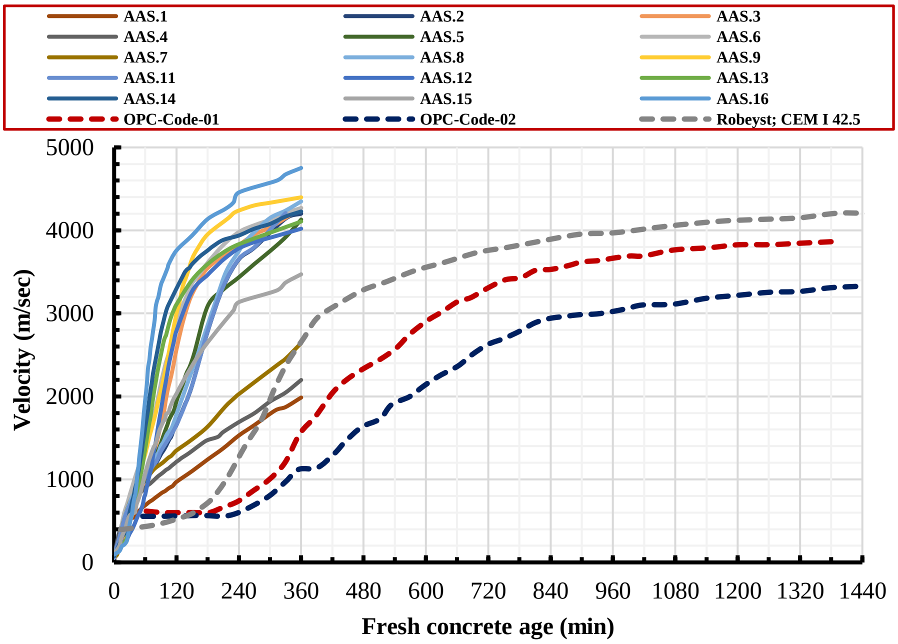

Fig. 19. Comparison of setting-time curves for OPC and slag-based geopolymer concrete.

5. Conclusions

In this study, the ultrasonic method was applied to assess the setting stages of slag-based geopolymer concrete at early ages. The experimental results indicate that this method can provide a comprehensive depiction of the polymerization process and the development of the microstructure of this type of concrete with a chosen composition.

All the ultrasonic velocity curves obtained (except those for samples containing 4 M sodium hydroxide (NaOH), which required more time to reach the final setting point) exhibited a similar three-phase pattern: an initial phase of very low, nearly constant velocity; a second phase with an abrupt increase in velocity; and a third phase during which the rate of increase in velocity slows after a few minutes. As in ordinary concrete, the initial setting time of the geopolymer mixtures was taken as the inflection point of this curve, and the final setting time as the onset of the third phase.

The results also show that slag-based geopolymer concretes set much faster than OPC concrete, with their polymerization reaction and final hardening occurring on average 6–8 times faster than those of OPC concrete. Furthermore, the initial and final setting times decrease as the molarity of the alkaline activator is increased: the alkaline hydroxide initially cleaves the Al–Si bonds and dissolves aluminum ions (which act as polymerization catalysts), and the addition of soluble sodium silicate results in the formation of a hydrated alkali aluminosilicate gel.

Raising the activator concentration from 4 M to 6 M dramatically shortens both the initial and final setting times, whereas a further increase to 8 M results in only a slight additional reduction. Similarly, in mixtures with a fixed NaOH molarity, increasing the overall alkaline solution-to-slag ratio from 0.4 to 0.5 accelerates slag activation and increases the heat of reaction, leading to shorter initial and final setting times for the fresh concrete. Increasing the slag content itself also accelerates the hydration reactions and further reduces the setting time, because the extra calcium in the slag greatly accelerates the process and promotes the rapid formation of C–S–H and C–A–S–H phases. In addition, using potassium hydroxide as the alkaline activator, compared with NaOH at the same molarity, markedly reduces the initial and final setting times of the fresh concrete, likely due to the chemical properties of the potassium ion.

Finally, the UPV method, used in conjunction with a Freshcon mold, is recommended as an appropriate test for assessing the setting times of slag-based geopolymer concrete. Although the rapid setting of geopolymer mixtures in volumetric applications may lead to the formation of cold joints and impose significant time constraints on molding processes, this property—by accelerating the rate of initial hardening—offers considerable advantages for the production of precast elements and the application of geopolymer shotcrete, particularly in tunnel rock support systems. Consequently, the high performance of geopolymer shotcrete justifies further in-depth evaluation in future research. Such studies should focus on critical aspects, including long-term durability and fire resistance. These investigations, which may involve advanced laboratory techniques such as thermomechanical analysis and numerical modeling using finite element methods, not only support global initiatives aimed at reducing greenhouse gas emissions in the construction industry but also contribute to advancing specialized knowledge in the field of geopolymer materials and their innovative applications in civil engineering.

Furthermore, the establishment of an independent standard specifically tailored to the setting behavior of geopolymers, coupled with comprehensive field validation of the UPV methodology under realistic curing and confining conditions, is crucial for the advancement of future research in this domain.

Statements & Declarations

Author contributions

Nader Sabeti: Conceptualization, Investigation, Methodology, Formal analysis, Resources, Writing - Original Draft, Writing - Review & Editing.

Funding

The authors received no financial support for the research, authorship, and/or publication of this article.

Data availability

The data presented in this study will be available on interested request from the corresponding author.

Declarations

The authors declare no conflict of interes.

References

[1] Nodehi, M., Taghvaee, V. M. Alkali-Activated Materials and Geopolymer: a Review of Common Precursors and Activators Addressing Circular Economy. Circular Economy and Sustainability, 2022; 2: 165-196. doi:10.1007/s43615-021-00029-w.

[2] Behforouz, B., Balkanlou, V. S., Naseri, F., Kasehchi, E., Mohseni, E., Ozbakkaloglu, T. Investigation of eco-friendly fiber-reinforced geopolymer composites incorporating recycled coarse aggregates. International Journal of Environmental Science and Technology, 2020; 17: 3251-3260. doi:10.1007/s13762-020-02643-x.

[3] Amran, M., Debbarma, S., Ozbakkaloglu, T. Fly ash-based eco-friendly geopolymer concrete: A critical review of the long-term durability properties. Construction and Building Materials, 2021; 270: 121857. doi:10.1016/j.conbuildmat.2020.121857.

[4] Turner, L. K., Collins, F. G. Carbon dioxide equivalent (CO2-e) emissions: A comparison between geopolymer and OPC cement concrete. Construction and Building Materials, 2013; 43: 125-130. doi:10.1016/j.conbuildmat.2013.01.023.

[5] Robbie, A. Global CO2 emissions from cement production. Earth System Science Data, 2017; 10: 195-217. doi:10.5194/essd-10-195-2018.

[6] Shi, C., Jiménez, A. F., Palomo, A. New cements for the 21st century: The pursuit of an alternative to Portland cement. Cement and Concrete Research, 2011; 41: 750-763. doi:10.1016/j.cemconres.2011.03.016.

[7] Matthes, W., Vollpracht, A., Villagrán, Y., Kamali-Bernard, S., Hooton, D., Gruyaert, E., Soutsos, M., De Belie, N. Ground Granulated Blast-Furnace Slag. In: N. De Belie, M. Soutsos, E. Gruyaert editors. Properties of Fresh and Hardened Concrete Containing Supplementary Cementitious Materials: State-of-the-Art Report of the RILEM Technical Committee 238-SCM, Working Group 4. Cham: Springer International Publishing; 2018. p. 1-53. doi:10.1007/978-3-319-70606-1_1.

[8] Davidovits, J. Geopolymers. Journal of thermal analysis, 1991; 37: 1633-1656. doi:10.1007/BF01912193.

[9] van Deventer, J. S. J., Provis, J. L., Duxson, P., Lukey, G. C. Reaction mechanisms in the geopolymeric conversion of inorganic waste to useful products. Journal of Hazardous Materials, 2007; 139: 506-513. doi:10.1016/j.jhazmat.2006.02.044.

[10] Palomo, A., Krivenko, P., Garcia-Lodeiro, I., Kavalerova, E., Maltseva, O., Fernández-Jiménez, A. A review on alkaline activation: new analytical perspectives. Materiales de Construcción, 2014; 64: e022. doi:10.3989/mc.2014.00314.

[11] Wang, Y., Zhang, S., Li, G., Shi, X. Effects of alkali-treated recycled carbon fiber on the strength and free drying shrinkage of cementitious mortar. Journal of Cleaner Production, 2019; 228: 1187-1195. doi:10.1016/j.jclepro.2019.04.295.

[12] Fernández-Jiménez, A., Palomo, A. Composition and microstructure of alkali activated fly ash binder: Effect of the activator. Cement and Concrete Research, 2005; 35: 1984-1992. doi:10.1016/j.cemconres.2005.03.003.

[13] White, C. E., Provis, J. L., Proffen, T., van Deventer, J. S. J. Molecular mechanisms responsible for the structural changes occurring during geopolymerization: Multiscale simulation. AIChE Journal, 2012; 58: 2241-2253. doi:10.1002/aic.12743.

[14] Lolli, F., Manzano, H., Provis, J. L., Bignozzi, M. C., Masoero, E. Atomistic Simulations of Geopolymer Models: The Impact of Disorder on Structure and Mechanics. ACS Applied Materials & Interfaces, 2018; 10: 22809-22820. doi:10.1021/acsami.8b03873.

[15] Dai, X., Aydin, S., Yardimci, M. Y., Lesage, K., De Schutter, G. Early age reaction, rheological properties and pore solution chemistry of NaOH-activated slag mixtures. Cement and Concrete Composites, 2022; 133: 104715. doi:10.1016/j.cemconcomp.2022.104715.

[16] Aiken, T. A., Kwasny, J., Sha, W., Tong, K. T. Mechanical and durability properties of alkali-activated fly ash concrete with increasing slag content. Construction and Building Materials, 2021; 301: 124330. doi:10.1016/j.conbuildmat.2021.124330.

[17] Fang, Y., Zhuang, K., Zheng, D., Guo, W. The Influence of Alkali Content on the Hydration of the Slag-Based Geopolymer: Relationships between Resistivity, Setting, and Strength Development. Polymers, 2023; 15: doi:10.3390/polym15030518.

[18] Taghvayi, H., Behfarnia, K., Khalili, M. The Effect of Alkali Concentration and Sodium Silicate Modulus on the Properties of Alkali-Activated Slag Concrete. Journal of Advanced Concrete Technology, 2018; 16: 293-305. doi:10.3151/jact.16.293.

[19] Ahmed, H. U., Mohammed, A. S., Mohammed, A. A., Faraj, R. H. Systematic multiscale models to predict the compressive strength of fly ash-based geopolymer concrete at various mixture proportions and curing regimes. PLOS ONE, 2021; 16: e0253006. doi:10.1371/journal.pone.0253006.

[20] Arularasi, V., Thamilselvi, P., Avudaiappan, S., Saavedra Flores, E. I., Amran, M., Fediuk, R., Vatin, N., Karelina, M. Rheological Behavior and Strength Characteristics of Cement Paste and Mortar with Fly Ash and GGBS Admixtures. Sustainability, 2021; 13: doi:10.3390/su13179600.

[21] Ansell, A. Investigation of shrinkage cracking in shotcrete on tunnel drains. Tunnelling and Underground Space Technology, 2010; 25: 607-613. doi:10.1016/j.tust.2010.04.006.

[22] Jameel, F., Sjölander, A., Ansell, A. Testing the in situ properties of wet-mix shotcrete at early age. ed. Boca Raton (FL): CRC Press; 2025.

[23] Aldawsari, S., Kampmann, R., Harnisch, J., Rohde, C. Setting Time, Microstructure, and Durability Properties of Low Calcium Fly Ash/Slag Geopolymer: A Review. Materials, 2022; 15: doi:10.3390/ma15030876.

[24] Gebregziabiher, B. S., Thomas, R. J., Peethamparan, S. Temperature and activator effect on early-age reaction kinetics of alkali-activated slag binders. Construction and Building Materials, 2016; 113: 783-793. doi:10.1016/j.conbuildmat.2016.03.098.

[25] Jiang, X., Zhang, Y., Xiao, R., Polaczyk, P., Zhang, M., Hu, W., Bai, Y., Huang, B. A comparative study on geopolymers synthesized by different classes of fly ash after exposure to elevated temperatures. Journal of Cleaner Production, 2020; 270: 122500. doi:10.1016/j.jclepro.2020.122500.

[26] Feng, X., Wang, Y., Li, L., Jiang, Z., Zhou, G., Wu, Q., Wang, T. Experimental investigation on physical properties and early-stage strength of ultrafine fly ash-based geopolymer grouting material. Construction and Building Materials, 2024; 441: 137526. doi:10.1016/j.conbuildmat.2024.137526.

[27] American Society for Testing and Materials (ASTM). ASTM C403/C403M-16: Standard Test Method for Time of Setting of Concrete Mixtures by Penetration Resistance. West Conshohocken (PA): ASTM International; 2016. doi:10.1520/C0403_C0403M-16.

[28] Lee, T., Lee, J. Setting time and compressive strength prediction model of concrete by nondestructive ultrasonic pulse velocity testing at early age. Construction and Building Materials, 2020; 252: 119027. doi:10.1016/j.conbuildmat.2020.119027.

[29] Li, Z., Alfredo Flores Beltran, I., Chen, Y., Šavija, B., Ye, G. Early-age properties of alkali-activated slag and glass wool paste. Construction and Building Materials, 2021; 291: 123326. doi:10.1016/j.conbuildmat.2021.123326.

[30] Sathiparan, N., Jayasundara, W. G. B. S., Samarakoon, K. S. D., Banujan, B. Prediction of characteristics of cement stabilized earth blocks using non-destructive testing: Ultrasonic pulse velocity and electrical resistivity. Materialia, 2023; 29: 101794. doi:10.1016/j.mtla.2023.101794.

[31] American Society for Testing and Materials (ASTM). ASTM C136/C136M: Standard Test Method for Sieve Analysis of Fine and Coarse Aggregates. West Conshohocken (PA): ASTM International; 2019. doi:10.1520/C0136_C0136M-14.

[32] American Society for Testing and Materials (ASTM). ASTM C33/C33M: Standard Specification for Concrete Aggregates. West Conshohocken (PA): ASTM International; 2018. doi:10.1520/C0033_C0033M-18.

[33] Zhang, H., Li, L., Long, T., Sarker, P. K., Shi, X., Cai, G., Wang, Q. The Effect of Ordinary Portland Cement Substitution on the Thermal Stability of Geopolymer Concrete. Materials, 2019; 12: doi:10.3390/ma12162501.

[34] Naghizadeh, A., Ekolu, S. Effect of different mixture parameters on the setting time of fly ash/rice husk ash-based geopolymer mortar. MATEC Web of Conferences, 2022; 361: 05001. doi:10.1051/matecconf/202236105001.

[35] American Society for Testing and Materials (ASTM). ASTM C191: Standard Test Method for Time of Setting of Hydraulic Cement by Vicat Needle. West Conshohocken (PA): ASTM International; 2000. doi:10.1520/C0191-21.

[36] British Standards Institution. BS 1881-203: Testing concrete recommendations for measurement of velocity of ultrasonic pulses in concrete. United Kingdom: BS Standard; 1986.

[37] British Standards Institution. BS EN 196-3: Methods of testing cement - Determination of setting times and soundness. United Kingdom: BS Standard; 2016.

[38] Reinhardt, H. W., Grosse, C. U. Continuous monitoring of setting and hardening of mortar and concrete. Construction and Building Materials, 2004; 18: 145-154. doi:10.1016/j.conbuildmat.2003.10.002.

[39] Huseien, G. F., Sam, A. R. M., Shah, K. W., Mirza, J., Tahir, M. M. Evaluation of alkali-activated mortars containing high volume waste ceramic powder and fly ash replacing GBFS. Construction and Building Materials, 2019; 210: 78-92. doi:10.1016/j.conbuildmat.2019.03.194.

[40] Xu, W., Tang, Z., Xie, Y., Long, G., Zhu, H., Kai, M., Peng, L., Wang, L., Zaland, S. Effect of synthesis parameters on the alkali activation reaction degree and the relationship between reaction degree and microstructure of fly ash-based geopolymers. Journal of Building Engineering, 2024; 93: 109874. doi:10.1016/j.jobe.2024.109874.

[41] Yang, C., Liu, J., Liu, L., Kuang, L., Zhang, S., Chen, Z., Li, J., Shi, C. Effects of different activators on autogenous shrinkage of alkali-activated slag cement. Construction and Building Materials, 2024; 446: 138018. doi:10.1016/j.conbuildmat.2024.138018.

[42] Mehdizadeh, H., Najafi Kani, E. Rheology and apparent activation energy of alkali activated phosphorous slag. Construction and Building Materials, 2018; 171: 197-204. doi:10.1016/j.conbuildmat.2018.03.130.

[43] Abdul Rahim, R. H., Rahmiati, T., Azizli, K. A., Man, Z., Nuruddin, M. F., Ismail, L. Comparison of Using NaOH and KOH Activated Fly Ash-Based Geopolymer on the Mechanical Properties. Materials Science Forum, 2015; 803: 179-184. doi:10.4028/www.scientific.net/MSF.803.179.

[44] Robeyst, N., Gruyaert, E., Grosse, C. U., De Belie, N. Monitoring the setting of concrete containing blast-furnace slag by measuring the ultrasonic p-wave velocity. Cement and Concrete Research, 2008; 38: 1169-1176. doi:10.1016/j.cemconres.2008.04.006.